Fermi surface investigation of the noncentrosymmetric superconductor α-PdBi

J. Klotz, T. A. Butcher, T. Förster, J. Hornung, I. Sheikin, P. Wisniewski, Anton Jesche, J. Wosnitza, D. Kaczorowski

Angaben zur Veröffentlichung / Publication details:

Klotz, J., T. A. Butcher, T. Förster, J. Hornung, I. Sheikin, P. Wisniewski, Anton Jesche, J. Wosnitza, and D. Kaczorowski. 2020. "Fermi surface investigation of the noncentrosymmetric superconductor α-PdBi." *Physical Review B* 101 (23): 235139. https://doi.org/10.1103/physrevb.101.235139.

Fermi surface investigation of the noncentrosymmetric superconductor α-PdBi

J. Klotz,[1] T. A. Butcher,[1,2,*] T. Förster,[1] J. Hornung,[1,2] I. Sheikin,[3] P. Wisniewski,[4] A. Jesche,[5] J. Wosnitza,[1,2] and D. Kaczorowski[4]

[1]*Hochfeld-Magnetlabor Dresden (HLD-EMFL) and Würzburg-Dresden Cluster of Excellence ct.qmat, Helmholtz-Zentrum Dresden-Rossendorf, 01328 Dresden, Germany*

[2]*Institut für Festkörper- und Materialphysik, Technische Universität Dresden, 01062 Dresden, Germany*

[3]*Laboratoire National des Champs Magnétiques Intenses (LNCMI-EMFL), CNRS, UGA, 38042 Grenoble, France*

[4]*Institute of Low Temperature and Structure Research, Polish Academy of Sciences, 50-950 Wrocław, Poland*

[5]*Experimentalphysik VI, Center for Electronic Correlations and Magnetism, Augsburg University, 86159 Augsburg, Germany*

(Received 17 March 2020; accepted 4 June 2020; published 16 June 2020)

The noncentrosymmetric superconductor α-PdBi is a candidate material for the realization of topological superconductivity. Here, we present a detailed de Haas–van Alphen (dHvA) study together with band-structure calculations within the framework of density functional theory. The rich dHvA spectra are a manifestation of the 13 bands that cross the Fermi energy E_F. We find excellent agreement between calculated and experimentally observed dHvA frequencies with moderately enhanced effective masses. One of the bands crossing E_F, the so-called α band, exhibits topological character with Weyl nodes lying 43 meV below E_F.

DOI: 10.1103/PhysRevB.101.235139

I. INTRODUCTION

Since several years, noncentrosymmetric (NCS) superconductors have attracted enormous research interest due to their unconventional physical properties [1,2]. The absence of an inversion center in the crystal lattice implies the occurrence of an intrinsic electric-field gradient that gives rise to a Rashba-type antisymmetric spin-orbit coupling (SOC) [2,3]. This effect lifts the spin degeneracy of electronic bands and a parity-mixed superconductivity may develop in consequence [4,5]. Most remarkably, it has recently been noticed that NCS superconductors with strong antisymmetric SOC provide an excellent platform for the realization of topological superconductivity (TSC) [6–8]. Such a material is a fully gapped bulk superconductor with topologically protected gapless states at the Fermi level [7,8]. In such a system, Majorana surface states with a nontrivial bulk Bogoliubov–de Gennes quasiparticle wave function can arise, which possess helical spin polarization locked to momentum. These are highly promising for the practical achievement of decoherence-robust qubits with the potential for application in quantum computing [9–12].

Amidst various candidates for TSC, the NCS compound α-PdBi is of unique interest. It crystallizes in an orthorhombic lattice and undergoes a structural transition upon cooling below 210 °C to a monoclinic structure of its own type (space group $P2_1$, No. 4) [13] and exhibits bulk type-II weak-coupling clean-limit superconductivity below $T_c = 3.7$K [14–20]. Strong SOC has been clearly evidenced experimentally by means of angle- and spin-resolved photoemission spectroscopy (ARPES) [21–24] as well as scanning tunneling spectroscopy (STS) [24,25]. Furthermore, both experimental techniques revealed the presence of a surface Dirac state located at about 700 meV below the Fermi level and this has been supported by first-principle band-structure calculations [21–25]. While the absence of a topologically nontrivial surface state in the immediate vicinity of the chemical potential rules out the possibility of TSC in parent α-PdBi with high likelihood, such effects might arise in this material upon tuning the Fermi level near the Dirac surface state. Proper electrical gating or surface engineering provide the means to achieve this [21].

In order to contrive an efficient route towards realization of TSC in α-PdBi, an in-depth investigation of its electronic structure is compulsory. Most recently, the Fermi surface of the compound has been characterized by means of de Haas–van Alphen (dHvA) oscillations [26]. These experiments revealed the presence of several Fermi-surface pockets, as did the spectroscopic measurements [21]. Most strikingly, one of the bands was found to bear signatures of a topologically nontrivial bulk state, which evaded detection in both ARPES and STS. This important finding may imply a nontrivial character of the superconducting order parameter associated with that particular Fermi-surface sheet, which in itself hints at TSC in the compound [27].

Motivated by the results reported in Ref. [26], we explored the multisheet Fermi surface (FS) of α-PdBi in more detail using the same experimental technique, namely, dHvA quantum-oscillation measurements performed at temperatures as low as 40 mK for various directions of the applied magnetic field. We were able to resolve very rich dHvA spectra for all field orientations. These contain numerous extremal orbits that are well reflected by our density-functional-theory (DFT) FS calculations. The experimentally determined band-resolved mass enhancement is moderate, which corresponds to the reported T_c of 3.7 K. One of the calculated bands shows

*Present address: School of Physics, Trinity College Dublin, Dublin 2, Ireland.

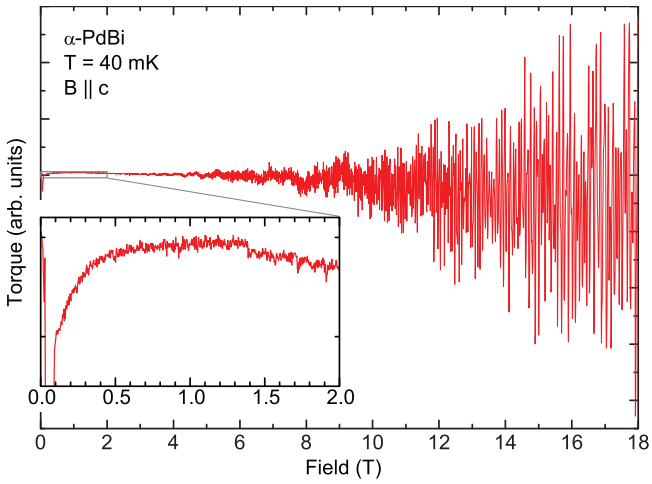

FIG. 1. Field-dependent torque signal of α-PdBi measured at 40 mK and the applied magnetic field $B \parallel c$. Inset: Zoom into the low-field region of the main panel.

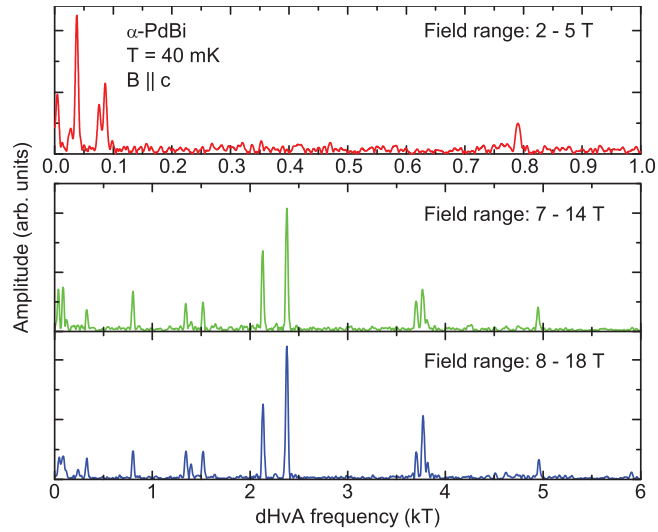

FIG. 2. dHvA frequency spectra obtained from the torque data shown in Fig. 1 for different field ranges. Note the different scaling of the frequency axes between the top panel and the two bottom panels.

nontrivial topology with Weyl nodes 43 meV below the Fermi energy E_F. In the following, we describe our experimental and calculated results in more detail.

II. EXPERIMENTAL DETAILS

Ultrahigh-quality single crystals of PdBi used in the present study were selected from the same batch as those studied in Ref. [21]. These were grown by a modified Bridgman method and characterized by means of x-ray diffraction, energy-dispersive x-ray spectroscopy, magnetic susceptibility, electrical resistivity, and heat-capacity measurements, as described before [21].

Angle-dependent quantum-oscillation measurements were performed using capacitive torque magnetometry, employing 50-μm-thick CuBe cantilevers. These experiments were conducted in a superconducting magnet system equipped with a top-loading dilution refrigerator reaching 18 T and 40 mK, respectively.

III. dHvA RESULTS

Figure 1 shows a typical torque signal for α-PdBi measured at 40 mK with the magnetic field B applied parallel to c. Note that throughout this paper, we use the $P112_1$ convention of the space group $P2_1$ (No. 4), i.e., the screw axis is parallel to c. This is consistent with the definition used by Yaresko *et al.* [28], but different from the convention used by Khan *et al.* [26]. The inset of Fig. 1 shows the data below 2 T in enlarged scale. A pronounced peak effect emerges near the superconducting upper critical field, which was estimated to be approximately 75 mT from specific-heat and STS measurements [19,25]. Quantum oscillations become visible above about 1.5 T and greatly increase in amplitude towards higher fields [29].

Figure 2 shows the corresponding dHvA frequency spectra, obtained by subtracting a third-order polynomial from the torque data and subsequently performing a Fourier transformation of the resulting data within the field range specified in the different panels of Fig. 2. Even in the lowest field range (2–5 T), clear dHvA frequency peaks are resolved. Towards higher magnetic fields, further peaks appear, reflecting the presence of several additional extremal orbits of FS sheets. The large number of dHvA frequencies evidence the existence of a rather evolved FS topology originating from many bands, as confirmed by our band-structure calculations below.

Figure 3 shows the temperature dependence of the dHvA oscillation amplitudes obtained for $B \parallel c$ between 3 and 6 T. The amplitudes clearly decrease with increasing temperature. As described by the Lifshitz-Kosevich formula, this reduction in amplitudes is proportional to $x/\sinh x$, where $x = \alpha T m^*/B$, with the effective cyclotron mass m^* and $\alpha = 2\pi^2 k_B m_e/(e\hbar) = 14.69$ T/K [30]. Here, we used the Boltzmann constant k_B, the electron charge e, and the reduced Planck constant $\hbar$. m^* represents the effective mass given

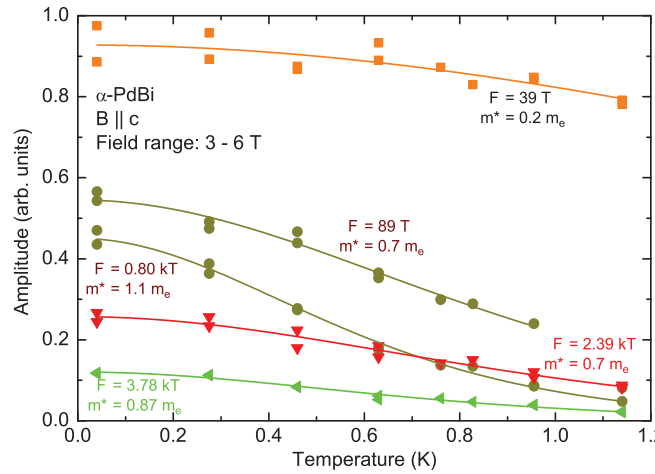

FIG. 3. Effective masses determined by fits of the Lifshitz-Kosevich formula (lines) to the temperature-dependent dHvA oscillation amplitudes (symbols).

TABLE I. Experimental and calculated dHvA frequencies and effective masses of α-PdBi for $B \parallel c$. The experimental masses were averaged over several different field ranges. See text for further information.

Experiment		FPLO calculation			λ
F (kT)	m^* (m_e)	Band	F (kT)	m_b (m_e)	$m^*/m_b - 1$
0.039	0.20(3)	333	0.031	0.14	0.4
0.089	0.67(3)	332	0.065	0.30	1.2
0.33	1.3(1)	329/330	0.33	0.67	0.9
0.80	1.1(1)	332	0.75	0.66	0.7
1.34	2.0(1)	332	1.18	0.88	1.3
1.40	1.1(1)				
1.52	1.1(1)				
2.13	0.65(2)	321/322	2.15	0.46	0.4
2.39	0.71(3)	323/324	2.46	0.50	0.4
3.78	0.87(3)	327	3.80	0.81	0.1
3.82	1.0(1)	325/326	3.86	0.70	0.4
4.95	1.5(1)	327	4.90	0.89	0.7
5.91	1.2(1)	329/330	5.92	1.10	0.1

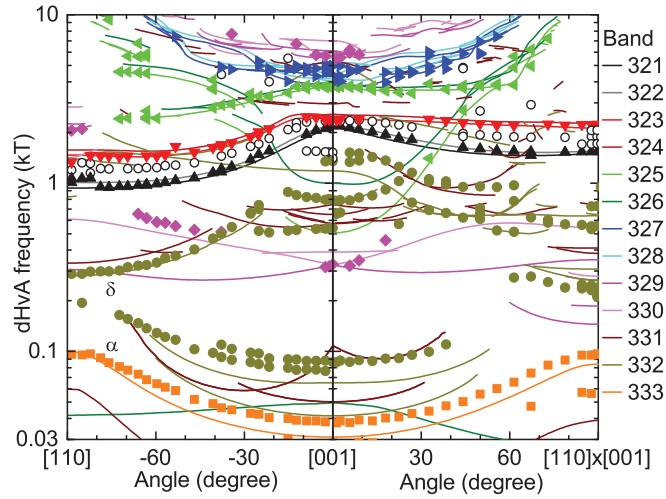

FIG. 4. Angular dependence of the experimentally observed dHvA frequencies (symbols) and of the calculated extremal Fermi-surface cross sections (lines) in α-PdBi. The line colors correspond to the band and FS colors shown in Fig. 5. Open symbols denote frequencies which could not clearly be assigned to a calculated frequency branch. Since spin-split bands in α-PdBi produce similar Fermi-surface sheets and, hence, similar dHvA frequencies, we assigned and color-coordinated the experimental data only to the pair of bands. α and δ label the frequency branches which were also observed by Khan *et al.* [26].

in multiples of the free electron mass m_e. By fitting this formula to the temperature dependence of the amplitudes, we obtain m^* as a fit parameter, with B being the average in inverse fields. Since the dHvA amplitude reduction of low-mass extremal orbits at higher field ranges is too small for a reasonable extraction of m^*, we use adapted field ranges for the analysis of m^*: 2–5, 3–6, 7–14, and 8–18 T. Within error bars, the effective masses of all extremal orbits investigated are not field dependent. Altogether, the effective masses are low, ranging from 0.20(3) to 2.0(1) m_e. An overview of experimentally determined effective masses is given in Table I, together with calculated band masses.

Next, we measure the angular dependence of the dHvA frequencies, rotating from $B \parallel c$ to $B \parallel [110]$ and from $B \parallel c$ to $B \parallel [110] \times [001]$ (i.e., the axis which is perpendicular to both [110] and [001]). All angles are measured rotating away from the crystallographic c axis. After carefully analyzing the frequency spectra for different field ranges and removing higher harmonics of fundamental dHvA frequencies, we obtain the angular dependence indicated by symbols in Fig. 4. The frequency branches α and δ reported in Ref. [26] are in excellent agreement with branches appearing in our experiments between $B \parallel c$ and $B \parallel [110]$. In addition, we also observe most of the frequency peaks reported for $\Theta = 70^\circ$ in Ref. [26]. Small deviations may arise due to the unknown in-plane angle in Ref. [26]. Besides these previously known dHvA orbits, several additional dHvA frequency branches occur in our experiments. Four of these appear at all angles and several more were only resolvable for a limited angular range. Due to the abundance of frequencies, different branches could only be assigned with the help of FS calculations, which we discuss below.

IV. FERMI-SURFACE CALCULATIONS

In order to determine the FSs that account for the experimentally detected dHvA frequencies, we conducted DFT calculations for α-PdBi using the FPLO code (Version 15.02-50) [31] with a fully relativistic formalism [32]. We chose the local density approximation of Perdew and Wang for the exchange-correlation potential [33]. As shown by Yaresko *et al.*, the correct determination of the band structure requires the primitive unit cell [28]. The structural parameters were set to the room-temperature data reported by Ionov *et al.* [28,34]. Altogether, there are eight inequivalent atomic sites in α-PdBi. This, coupled with the low crystal symmetry brings about computationally intensive calculations. While a comparatively fine $24 \times 24 \times 24$ k mesh could be used for calculating the self-consistent density, we were restricted to an only 4 times denser grid to compute the FSs [35].

Figure 5(a) shows the calculated band structure of α-PdBi. We find a total of 13 bands crossing the Fermi energy, consistent with the results reported in Ref. [26]. The non-centrosymmetric crystal structure leads to a finite spin-orbit coupling (SOC), which removes the spin degeneracy of the bands except for some symmetry lines in the Brillouin zone (BZ). On the one hand, the energy scale of the splitting is fairly small compared to the energy scale of the band widths, leading to pairwise similar bands 321 and 322, 323 and 324, etc. On the other hand, due to the high nuclear charge of the Bi atoms, SOC is comparatively strong, amounting to up to about 0.2 eV, depending on the location in the BZ and the bands. Hence, most of the FS sheets corresponding to spin-split bands are very much alike, as shown in Fig. 5(c). However, the energy splitting greatly changes the FS shapes of bands which are close to the Fermi energy in extended regions of the BZ. For example, band 331 crosses the Fermi energy multiple times along Γ-Y-C, whilst band 332 does not cross it

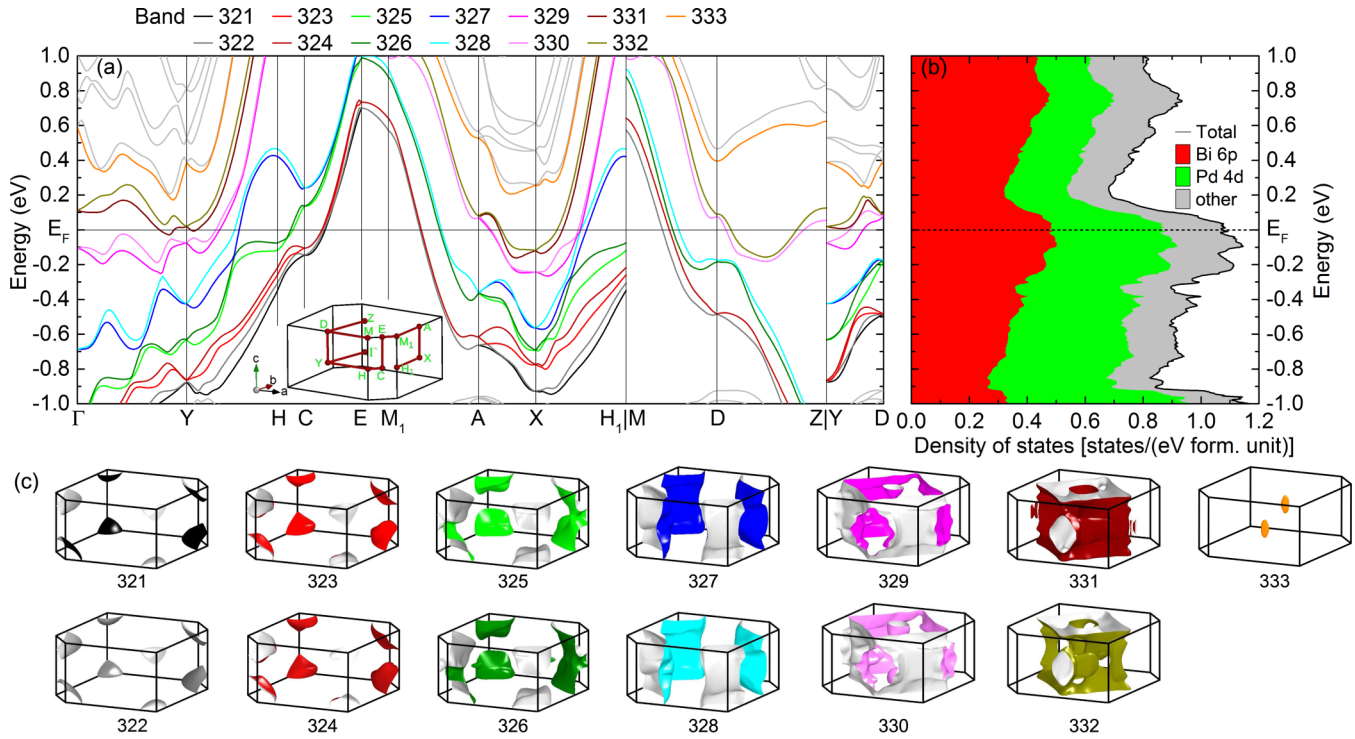

FIG. 5. (a) Calculated band structure of α-PdBi along lines of the Brillouin zone indicated in the sketch. Along the symmetry lines E-M_1-A and M-D-Z, SOC is zero, leading to degeneracy of the bands 321/322, 323/324, etc. Note that band 333 crosses the Fermi energy only outside the lines shown here. A detailed investigation of the Fermi-energy crossing of bands 331 to 333 is shown in Fig. 6. (b) Corresponding density of states. The shaded areas mark contributions of different atomic orbitals. (c) Calculated FSs. The colors correspond to those of the conduction bands in panel (a).

at all along these lines. Thus, the FSs of the bands 331 and 332 differ significantly: Band 331 possesses two additional tiny FS pockets, whereas a larger part of the FS sheet of band 332 around the X point is completely separated. Similarly, band 326 produces an additional small pocket compared to band 325. Band 333 only dips below the Fermi energy in a small region outside of the lines shown in Fig. 5(a), while band 334 remains entirely above the Fermi level. The crossings of bands 332 and 333 are discussed further below.

The calculated density of states (DOS) is shown in Fig. 5(b). The DOS at the Fermi level is $D(E_F) = 1.1$ states/(eV formula unit). Using $\gamma_{\text{calc}} = \pi^2 k_B^2 D(E_F)/3$, we determine a Sommerfeld coefficient of $\gamma_{\text{calc}} = 2.6$ mJ/(mol K^2). An effective-mass enhancement due to many-body effects is implied by the discrepancy between the experimental value of $\gamma = 4$ mJ/(mol K^2) [14] and the theoretically obtained one. From $\lambda_\gamma = \gamma/\gamma_{\text{calc}} - 1$, we obtain a moderate mass enhancement of $\lambda_\gamma = 0.5$. This includes the averaged mass enhancement due to electron-phonon and electron-electron interactions.

Every fundamental dHvA frequency F is related to an extremal cross section S of a FS sheet according to the Onsager relation: $F = \hbar S/(2\pi e)$ [30]. Thus, we are able to calculate theoretical dHvA frequencies from the FS sheets we obtained [Fig. 5(c)]. Figure 4 shows the comparison between the experimental and theoretical dHvA frequencies. The similarity of the spin-split bands manifests itself in their FS sheets and corresponding extremal cross sections in turn. Therefore, we assigned some of the experimental data to the pair of bands. Furthermore, the multitude of calculated cross sections means that some of the experimental frequencies cannot be allocated to calculated branches unambiguously.

Each of the simply connected pockets of bands 321–324 produce a single-frequency branch which spans all angles. These branches are well reproduced by the experiment. Between the data points of bands 321/322 and 323/324, we find additional dHvA frequencies in the experimental data (open circles in Fig. 4). Since these pairs of bands come very close in some parts of the BZ, for example, along the line M_1-A [see Fig. 5(a)], electrons can tunnel between the two bands. Consequently, magnetic breakdown is a likely reason for the appearance of the additional frequencies observed in experiments [30]. The hourglasslike shape of the FSs of bands 325/326 causes large changes of the related frequency branches when rotating away from the c axis, which become even more pronounced for the corrugated cylindrical FS sheets of bands 327/328. These calculated frequencies are also in very good agreement with experimental data.

Bands 329–332 produce complicated three-dimensional FS sheets with multiple connections. Not all of the calculated extremal cross sections were found experimentally for these sheets. The strong curvature of the FS sheets, which causes a reduction of the dHvA oscillation amplitudes [30], is the most likely reason for the missing dHvA frequencies. Furthermore, the comparatively coarse k mesh we used for the FS calculations may have been unable to resolve some fine details of the FSs [36]. Additionally, bands 329 and 330 feature a small pocket around the Z point, which corresponds

to frequency branches between 0.3 and 1 kT. These were only partially confirmed experimentally. In some cases, the Fourier spectra show double-peak structures (Fig. 2). These cannot be caused by spin splitting, since spin degeneracy is lifted by SOC, but may be due to twinning. For α-PdBi with noncentrosymmetric crystal structure, such twinning is hardly avoidable, as discussed in more detail in Refs. [24,25]. Finally, band 333 only crosses the Fermi level near the $k_z = 0$ plane of the BZ. This crossing is outside of the symmetry lines shown in Fig. 5(a) and yields small FS pockets. The corresponding frequency branch, identical to the α frequency reported in Ref. [26], was found at all investigated angles.

Using the assignments of the calculated extremal FS cross sections and experimental dHvA frequencies, we calculated the band masses m_b, and compared them to the experimental effective masses m^*, as shown in Table I. This allows us to estimate the band-resolved mass-enhancement factors, $\lambda = m^*/m_b - 1$. The values for λ lie between 0.1 and 1.3, which is in good agreement with the mass enhancement estimated from specific-heat data, $\lambda_\gamma = 0.5$ (see above). This estimate comprises the averaged λ over all bands and orientations. A large variation in the orientation- and band-resolved mass-enhancement factors is well known from other superconductors [37].

In Ref. [26], the frequency α, related to pocket 333, was reported to possess a nontrivial Berry phase, as extracted from a phase analysis of the dHvA oscillation. In our experiment we cannot safely determine the phase of the α oscillation due to the interference from the large number of other frequencies. In particular, we detected a neighboring low frequency at many angles, as can be seen in the upper panel of Fig. 2 as a side peak of the α frequency at 39 T, which can cause a large phase shift due to beatings. It is noteworthy that even a correct determination of the phase does not allow for conclusive statements on the existence of a Berry phase. A recent theory work by Alexandradinata *et al.* analyzes this in detail [38].

Nevertheless, it is still possible to further investigate the band structure of PdBi in the region where band 333 crosses the Fermi energy. For the pocket 333, we find a linear band crossing at $\mathbf{k_0} = (k_{x0}, k_{y0}, k_{z0}) = (0.399\,706, 0.056\,504, 0) \cdot 2\pi/a$, 43 meV below the Fermi energy, as shown in Fig. 6 [39]. This linear band crossing is a Weyl node and renders its surrounding FS sheet topologically nontrivial, which appears to support the suggested presence of topological states given in Refs. [26,42]. Note that the linear crossing is symmetry protected in the $k_z = 0$ plane, whereas the k_{x0} and k_{y0} positions are subject to numerical uncertainty. Furthermore, the twofold symmetry of the crystal structure is imparted on the band structure, producing a second Weyl node at $(-k_{x0}, -k_{y0}, 0)$.

It remains, however, questionable whether these Weyl nodes have any decisive effect on transport or other macroscopic electronic properties in α-PdBi. The energetic distance of the Weyl nodes from the Fermi energy (43 meV) seems to be too large to influence such properties even at room temperature. In addition, the linear dispersion is only found over a very limited energy range and only in one out of the 13 bands crossing E_F. Close to E_F, the dispersion of band 333 is much more curved and far from linear and the partial DOS resulting from this band contributes only about 0.23% to the total DOS.

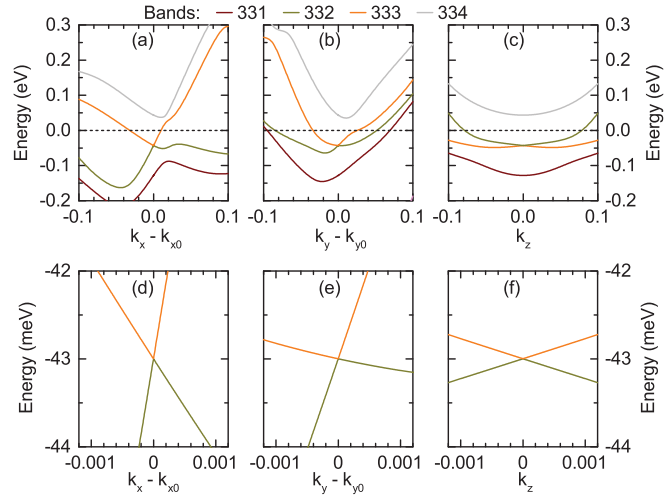

FIG. 6. Band structure of α-PdBi in the vicinity of the Weyl node at $\mathbf{k_0} = (k_{x0}, k_{y0}, k_{z0}) = (0.399\,706, 0.056\,504, 0)2\pi/a$. The cuts are running parallel to the (a) k_x, (b) k_y, and (c) k_z directions. The band colors are identical to those used in Fig. 5(a). Panels (d), (e), and (f) are zooms into panels (a), (b), and (c), respectively. In these zoomed images, we used a fine k spacing of steps in the range $|\mathbf{k} - \mathbf{k_0}| \leqslant 10^{-3}$ in order to show that the crossing is indeed nearly linear in all directions.

V. CONCLUSIONS

We performed a comprehensive dHvA study of the noncentrosymmetric superconductor α-PdBi. The dHvA results agree very well with FPLO DFT calculations. Altogether, 13 bands cross the Fermi energy leading to rich dHvA spectra. All observed FS sheets reveal rather small effective masses (2.0 m_e or less). Their moderate mass enhancement is in line with the average value of 0.5, which was estimated from specific-heat data and corresponds to the observed T_c of 3.7 K. One of the 13 bands, the so-called α band with the smallest extremal area, shows topologically nontrivial Weyl points 43 meV below the Fermi energy. Whether the electrons in this band give rise to topological superconductivity seems unlikely, but merits further study.

ACKNOWLEDGMENTS

We thank H. Rosner for helpful discussions. The work was supported by the Deutsche Forschungsgemeinschaft (DFG) through the Würzburg-Dresden Cluster of Excellence on Complexity and Topology in Quantum Matter–*ct.qmat* (EXC 2147, Project No. 390858490), by the ANR-DFG under Grant Fermi-NESt, by Grant No. JE748/1, and by Hochfeld-Magnetlabor Dresden (HLD) at HZDR, member of the European Magnetic Field Laboratory (EMFL). P.W. and D.K. were supported by the National Science Centre (Poland) under Grant No. 2015/18/A/ST3/00057.

[1] M. Sigrist and K. Ueda, Rev. Mod. Phys. **63**, 239 (1991).

[2] E. Bauer and M. Sigrist, *Non-Centrosymmetric Superconductors: Introduction and Overview* (Springer, New York, 2012).

[3] S. Yip, Annu. Rev. Condens. Matter Phys. **5**, 15 (2014).

[4] L. P. Gor'kov and E. I. Rashba, Phys. Rev. Lett. **87**, 037004 (2001).

[5] M. Smidman, M. B. Salamon, H. Q. Yuan, and D. F. Agterberg, Rep. Prog. Phys. **80**, 036501 (2017).

[6] X.-L. Qi and S.-C. Zhang, Rev. Mod. Phys. **83**, 1057 (2011).

[7] M. Z. Hasan and C. L. Kane, Rev. Mod. Phys. **82**, 3045 (2010).

[8] A. P. Schnyder, S. Ryu, A. Furusaki, and A. W. W. Ludwig, Phys. Rev. B **78**, 195125 (2008).

[9] A. Y. Kitaev, Phys.-Usp. **44**, 131 (2001).

[10] D. A. Ivanov, Phys. Rev. Lett. **86**, 268 (2001).

[11] F. Wilczek, Nat. Phys. **5**, 614 (2009).

[12] M. Sato and S. Fujimoto, Phys. Rev. B **79**, 094504 (2009).

[13] Y. C. Bhatt and K. Schubert, J. Less-Common Met. **64**, P17 (1979).

[14] B. Joshi, A. Thamizhavel, and S. Ramakrishnan, Phys. Rev. B **84**, 064518 (2011).

[15] M. Mondal, B. Joshi, S. Kumar, A. Kamlapure, S. C. Ganguli, A. Thamizhavel, S. S. Mandal, S. Ramakrishnan, and P. Raychaudhuri, Phys. Rev. B **86**, 094520 (2012).

[16] K. Matano, S. Maeda, H. Sawaoka, Y. Muro, T. Takabatake, B. Joshi, S. Ramakrishnan, K. Kawashima, J. Akimitsu, and G. Zheng, J. Phys. Soc. Jpn. **82**, 084711 (2013).

[17] L. Jiao, J. L. Zhang, Y. Chen, Z. F. Weng, Y. M. Shao, J. Y. Feng, X. Lu, B. Joshi, A. Thamizhavel, S. Ramakrishnan, and H. Q. Yuan, Phys. Rev. B **89**, 060507(R) (2014).

[18] X. B. Yan, Y. Xu, L. P. He, J. K. Dong, H. Cho, D. C. Peets, J.-G. Park, and S. Y. Li, Supercond. Sci. Technol. **29**, 065001 (2016).

[19] D. C. Peets, A. Maldonado, M. Enayat, Z. Sun, P. Wahl, and A. P. Schnyder, Phys. Rev. B **93**, 174504 (2016).

[20] S. Ramakrishnan, B. Joshi, and A. Thamizhavel, Philos. Mag. **97**, 3460 (2017).

[21] M. Neupane, N. Alidoust, M. M. Hosen, J.-X. Zhu, K. Dimitri, S.-Y. Xu, N. Dhakal, R. Sankar, I. Belopolski, D. S. Sanchez, T.-R. Chang, H.-T. Jeng, K. Miyamoto, T. Okuda, H. Lin, A. Bansil, D. Kaczorowski, F. Chou, M. Z. Hasan, and T. Durakiewicz, Nat. Commun. **7**, 13315 (2016).

[22] H. Lohani, P. Mishra, A. Gupta, V. P. S. Awana, and B. R. Sekhar, Phys. C (Amsterdam, Neth.) **534**, 13 (2017).

[23] S. Thirupathaiah, S. Ghosh, R. Jha, E. D. L. Rienks, K. Dolui, V. V. Ravi Kishore, B. Büchner, T. Das, V. P. S. Awana, D. D. Sarma, and J. Fink, Phys. Rev. Lett. **117**, 177001 (2016).

[24] H. M. Benia, E. Rampi, C. Trainer, C. M. Yim, A. Maldonado, D. C. Peets, A. Stöhr, U. Starke, K. Kern, A. Yaresko, G. Levy, A. Damascelli, C. R. Ast, A. P. Schnyder, and P. Wahl, Phys. Rev. B **94**, 121407(R) (2016).

[25] Z. Sun, M. Enayat, A. Maldonado, C. Lithgow, E. Yelland, D. C. Peets, A. Yaresko, A. P. Schnyder, and P. Wahl, Nat. Commun. **6**, 6633 (2015).

[26] M. A. Khan, D. E. Graf, I. Vekhter, D. A. Browne, J. F. DiTusa, W. A. Phelan, and D. P. Young, Phys. Rev. B **99**, 020507(R) (2019).

[27] V. Barzykin and L. P. Gor'kov, Phys. Rev. B **76**, 014509 (2007).

[28] A. Yaresko, A. P. Schnyder, H. M. Benia, C.-M. Yim, G. Levy, A. Damascelli, C. R. Ast, D. C. Peets, and P. Wahl, Phys. Rev. B **97**, 075108 (2018).

[29] The small anomaly appearing at about 1.4 T (inset of Fig. 1) is an artifact of the measurement.

[30] D. Shoenberg, *Magnetic Oscillations in Metals* (Cambridge University, Cambridge, England, 1984).

[31] K. Koepernik and H. Eschrig, Phys. Rev. B **59**, 1743 (1999).

[32] H. Eschrig, M. Richter, and I. Opahle, in *Relativistic Electronic Structure Theory: Part 2. Applications*, edited by P. Schwerdtfeger, Theoretical and Computational Chemistry Vol. 14 (Elsevier, Amsterdam, 2004), pp. 723–776.

[33] J. P. Perdew and Y. Wang, Phys. Rev. B **45**, 13244 (1992).

[34] V. M. Ionov, N. A. Tomilin, A. E. Prozorovskii, A. N. Klimenko, Y. V. Titov, S. G. Zhukov, and G. V. Fetisov, Sov. Phys. Crystallogr. **34**, 496 (1989).

[35] For other materials with simpler crystal and band structure, FS calculations on up to 10 times denser grids are straightforward.

[36] The logarithmic frequency axis in Fig. 4 leads to a seemingly larger deviation between experimental and calculated dHvA frequencies for the low-frequency bands 332 and 333. However, in absolute numbers this difference is only 24 and 8 T, respectively. These values should be compared to the total area of the first Brillouin zone which corresponds to about 13100 T. See also Ref. [39].

[37] B. Bergk, V. Petzold, H. Rosner, S.-L. Drechsler, M. Bartkowiak, O. Ignatchik, A. D. Bianchi, I. Sheikin, P. C. Canfield, and J. Wosnitza, Phys. Rev. Lett. **100**, 257004 (2008).

[38] A. Alexandradinata, C. Wang, W. Duan, and L. Glazman, Phys. Rev. X **8**, 011027 (2018).

[39] Although modern DFT calculations show a high degree of reproducibility, they are all based on approximations. Therefore, differences between results using different codes and differences from experimental data are expected. For a deeper discussion of this DFT challenge, see Refs. [40,41]. This means for the values given for the position of the Weyl node, they are precise only for the used approximation and code, but may be off from experimental data by some amount. In the present case, where the experimental FS pocket of band 333 is larger by about 20% than calculated, the Weyl node might be even further away from the Fermi energy.

[40] T. Förster, I. Kraft, I. Sheikin, A. D. Bianchi, J. Wosnitza, and H. Rosner, J. Phys.: Condens. Matter **32**, 025503 (2020).

[41] K. Lejaeghere *et al.*, Science **351**, aad3000 (2016).

[42] In Ref. [26], no detailed analysis of the α-band dispersion relation is given. The presence of topological states is concluded only from the phase analysis of the dHvA oscillations.